ACS OMEGA

Open Access

http://pubs.acs.org/journal/acsodf

Article

Atomistic Analysis of Sulphonamides as a Microbial Influenced Corrosion (MIC) Inhibitor

Mohammad Asif, N.V. Saidileep Korlapati, Faisal Khan,* Kelly Hawboldt, and Susan Caines

Cite This: *ACS Omega* 2024, 9, 38722−38732

Read Online

ACCESS | Metrics & More | Article Recommendations | Supporting Information

ABSTRACT: Four sulfonamide-type microbial inhibitors were studied using density functional theory (DFT) to assess their effectiveness in controlling microbial corrosion. The experimental techniques (FTIR, SEM, EIS, EFM, and AFM) are beneficial for measuring properties such as chemical composition, bond formation, electrochemical behavior, and surface topography; however, DFT can be useful as a new method for understanding microbial corrosion. Sulfacetamide (SFC), sulfamerazine (SFM), sulfapyridine (SFP), and sulfathiazole (SFT) uniformly adsorb onto the iron surface and block the active site, reducing the corrosion rate. To study the effect on microbial activity, a 0.6 eV electric field was applied. The absolute increase in the interaction energy indicates that sulfonamides are effective microbial inhibitors. Electronic SFC, SFM, SFP, and SFT descriptors agree with the experimental inhibition efficiency. The shift of the density of state (DOS) toward a low energy level for sulfonamides indicates the stabilization of these molecules at the Fe (100) surface. The population analysis combined with atomic and molecular parameters further explains the anticorrosive mechanism of sulphonamides.

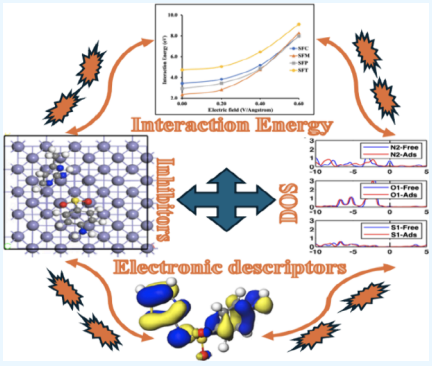

1. INTRODUCTION

Iron and its alloys are extensively used in various industries, including the oil and gas industry, due to their excellent mechanical properties. Nonetheless, they are prone to deterioration due to direct contact with corrosive materials and their surroundings. Applying inhibitors such as sulphonamides is one of the most cost-effective and useful methods of protecting iron surfaces from degradation.[1,2]

It is well-known that artificial organic long-chain compounds with *O, S,* and *N* atoms are well-matched as inhibitors due to high electron density and strong basicity.[3,4] These organic compounds can transfer electrons to unoccupied d-orbitals of an iron surface (Fe100) or to various sites (hollow, bridge, and top) in the layer of an oxide ("passive") film to form coordinate or covalent bonds. These compounds may also accept valence electrons from the iron surface by providing their antibonding orbitals to make feedback bonds and, therefore, are commonly used in corrosion inhibition.[5]

Sulphonamides are drugs primarily used to treat infections due to Gram-positive microbes, certain fungi, and some protozoa. While the influx of antibiotics has reduced the application of the sulfonamides, they still have a small but significant space in therapeutic resources for numerous physicians. Further therapeutic applications of sulfonamides include their use as diuretic and hypoglycemic agents. Those compounds have functional adsorption groups, e.g., $-NH_2$ group, $-SO_2-NH-$group, and aromatic rings *O* and/or *N* heteroatoms. These compounds are strongly basic and, therefore, can be highly soluble in the acid medium.[6]

Many experimental procedures, e.g., weight loss technique, potentiodynamic polarization, electrochemical impedance spectroscopy (EIS), and electrochemical frequency modulation (EFM), have been used to test the inhibition efficiency of different organic and inorganic compounds on various metal surfaces.[7−23] Other analytical methods, such as scanning electron microscopy (SEM),[24−26] atomic force microscopy (AFM),[19,26] cyclic voltammetry,[27] and FTIR analysis,[28,29] have been used to explore the component's composition, various bond formation, and some properties related to protective layer structure. Experimental techniques roughly assess the inhibition efficiency; these are usually expensive, time-cumbersome, and difficult to provide a strong anticorrosive mechanism at the atomistic level.[30] Tremendous literatures on theoretical findings of corrosion inhibitors relied on techniques such as the DFT and molecular dynamics have been shown to match experiments to this regard.[31−37] The advantage of the DFT is that it can be used for large systems with reasonable computations. Loutfy et al.[38] studied adsorption behavior and inhibition mechanism of synthesized bis-azo dye applying molecular dynamics (MD). In a different study, Sourav et al.[39] performed MD simulations for the corrosion inhibition of

Received: May 15, 2024
Revised: July 26, 2024
Accepted: July 30, 2024
Published: September 3, 2024

quinazolinone and pyrimidinone compounds to mimic the real environment.

Nevertheless, details of this occurrence (bond formation and charge distribution) and what controls the strength of the interaction are known poorly.[31] Moreover, the inhibitive mechanism of sulphonamides is unclear; for instance, minor variations in the configuration of molecular structures could significantly impact their efficacy.[30]

Approximately 20% of the total corrosion occurs due to microbes in the oil and gas industry.[40] Microbial activity in the airline industry is also related to the deterioration of the fuel storage tanks.[41] The electron transfer is necessary between microbes and metal/*Fe* (100) surface.[42] The DFT at the electronic level offers a pathway to understand a very complex transformation, e.g., microbial corrosion;[43,44] however, the mechanism of the electron transfer to microbes is still unknown. An electric field at the DFT level could resemble the microbes on the metal surface and subsequently the adsorption mechanism of sulphonamides. However, this needs a series of experiments, as discussed in our previous work.[45] Details of the exact phenomenon of microbially influenced corrosion are more complex as abiotic and biotic corrosion occur simultaneously.[46]

The quantum calculations and experimental inhibition efficiency (%IE) of sulphonamide inhibitors are often linked with correlation analysis and indicate that it is closely related to the highest occupied molecular orbital (HOMO), lowest unoccupied molecular orbital (LUMO), hardness, dipole moment, polarizability, and electronic charges.[47] The %IE will increase with an increase in HOMO and a reduction in the energy gap (ΔE_{gap}). Excellent corrosion inhibitors have less energy gaps that offer electrons to the unoccupied d atomic orbital of iron and accept free electrons from iron.[48,49] Because wave functions of HOMO and LUMO for the inhibitors of medium-sized ΔE_{gap} are combined with ease, the inhibitors are rapidly polarized and require little energy to be excited.[50,51] Thus, the calculated low ΔE_{gap} promotes chemical reactivity of the inhibitors toward Fe (100) and therefore their ability as a corrosion inhibition candidate.

The experimental studies for inhibition due to SFC, SFM, SFP, and SFT are well-established for corrosion in acidic media; however, its effect on microbial corrosion and protection from the pit nucleation is still, to the best of our knowledge, an important, unrevealed question.

This work studies the adsorption of SFC, SFM, SFP, and SFT in the molecular and dissociative form at the *Fe* (100) surface. Based on the quantum chemical calculations, we optimize the Fe (100) surface model covered with sulphonamides. This is the first step in the atomistic understanding of microbial corrosion with an electric field changing from 0 to 0.6 V/Å. This work aims to illustrate the details of bond formation and determine the strength of the sulfonamide's interaction at the *Fe* (100) surface, including the electronic density and charge distribution. The tilt angle of the molecules/fragment at the *Fe* (100) surface is also explored. The negative sign of the HOMO and other thermodynamic parameters (interaction energy) suggests that the data resulting supports the physical/chemical interaction mechanism.

2. METHODOLOGY

This study has implemented the DFT[52−55] methodology. The study used generalized gradient approximation with the Perdew−Burke−Ernzerhof (GGA-PBE)[56] functional applied to DMol3[57] and CASTEP[58] modules in the BIOVIA Materials Studio 2020 platform. PBE incorporates a density gradient to account for the electron inhomogeneity in the system. The modules used in this work are shown in Figure 1. The DMol3

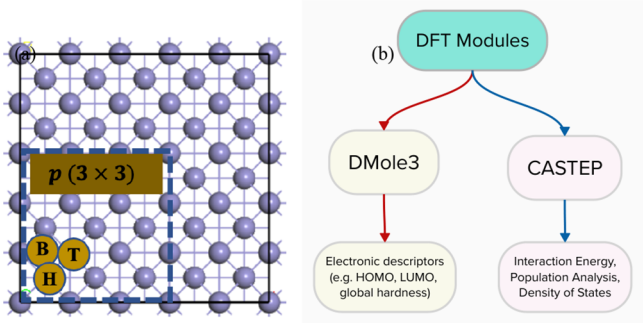

Figure 1. (a) Square 2D cell showing various sites. Each blue apex shows an iron atom in Fe (100). (b) Properties of the sulfonamides calculated from the various modules.

module was applied for the calculation of frontier molecular orbitals (HOMO and LUMO) of sulfonamides and related properties (ΔE_{gap}, absolute electronegativity, global hardness, and so forth). However, the CASTEP module is applied to calculate the interaction energy and electronic properties of the sulphonamides adsorbing at the Fe (100) surface.

2.1. DMol3. DMol3 accounts for a Fermi occupation scheme (electronic technique appropriate for the covalent systems) or a thermal occupation scheme (appropriate for metals), often required for converging electronic density.[59]

The double numerical plus polarization (DNP) is applied as a basis set (illustration of electrons in quantum state), which retains the d-type polarization function to heavy atoms (*Fe*) and p-type polarization functions to H_2 atoms; this provides improved precision by reducing the basis set superposition error (BSSE) relative to Gaussian 6-31G (d, p).[60,61] All the atoms were subjected to optimization until convergence in cutoff energy, force, and displacement reached 1.0×10^{-6} Ha (2.720×10^{-5} eV), 0.001 Ha/Å (0.0272 eV/Å), and 0.005 Å, respectively.

The work function of each slab is obtained using eq 1.

$$\varnothing_{slab} = E_{vacuum} - E_{Fermi} \quad (1)$$

where E_{vacuum} is the vacuum local potential energy, and E_{Fermi} is the Fermi level.

The work functions for the two, three, and four layers of the Fe (100) slabs are calculated as 0.142 Ha (3.86 eV), 0.145 Ha (3.95 eV), and 0.147 Ha (4.00 eV), respectively.

2.2. CASTEP. The four-layer iron slab with 5 × 5 supercells with 100 atoms was applied for the first principal calculations. This model is well-tested, including our previous work[62] and other people's work,[63,64] for quantum chemical calculations. The work function calculated from DMol3 in this work also shows that selecting four layers is better. The space (vacuum) above the slab was set to 25 Å in the normal direction to give ample space between cleaved surfaces to minimize interaction. We had selected the Gamma k-point due to the large slab size. To check the model accuracy, we performed a convergence test of total energy for the *Fe* (100) slab with 2 × 2 × 1 k points using the same basis sets. The error in total energy (Or interaction energy) is less than 0.01 eV. The cutoff energy for ultrasoft pseudopotential was set to 400 eV.

https://doi.org/10.1021/acsomega.4c04651
ACS Omega 2024, 9, 38722−38732

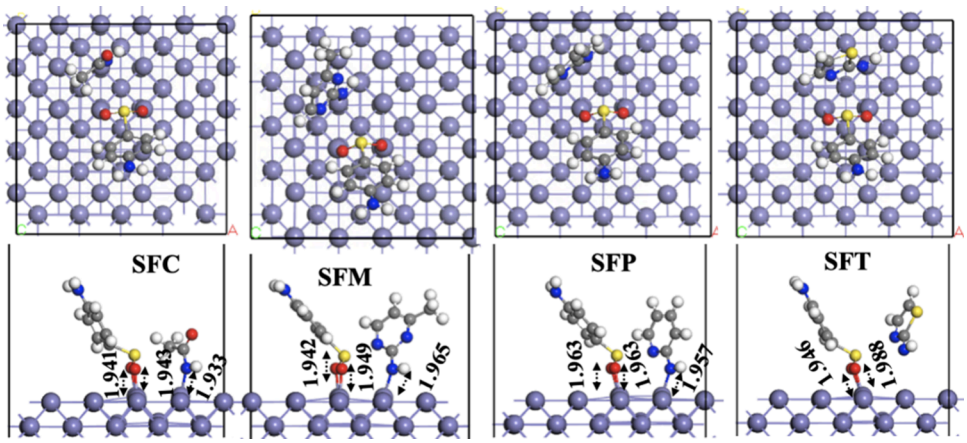

Figure 2. Top and side views for relaxed structure of the dissociative adsorption of the SFC, SFM, SFP, and SFT molecules at the Fe (100) surface using the CASTEP module at the DFT + D level. In the neutral molecule, the red is *O* atoms. The yellow is *S* atoms. The light gray is *C* atoms. The dark blue is *N* atoms. The light blue is *Fe* atoms, and the white is *H* atoms. The bond lengths are in Å.

The optimization of the Fe (100) slab is performed applying spacing for 10 × 10 × 10 of the bulk iron with the fine setting of Monkhorst−Pack k-point Brillouin zone sampling.[65] The estimated lattice constant for the BCC iron was $a = b = c =$ 2.812 Å after using the ultrasoft pseudopotential by an error of 1.88% related to the experimental value of 2.866 Å[66] and is in excellent agreement.

The interaction energy of the inhibitors is estimated by the following expression:[67]

$$E_{int} = [E_{complex} - (E_{slab} + E_{inhibitor})] \quad (2)$$

where $E_{complex}$ is the energy of the inhibitor/iron slab in the adsorbed state, E_{slab} is the energy of clean Fe (100), and $E_{inhibitor}$ is the energy of the inhibitor in an isolated state. Equation 2 is also used to calculate adsorption energy.

Both module functionals (DMole3 and CASTEP) performed well during calculations, although CASTEP removes the BSSE due to the plane wave. All the atoms were subjected to optimization until convergence in cutoff energy, force, stress, and displacement reached 2.0 × 10^{-6} eV, 0.02 eV/Å, 0.1 GPa, and 0.002 Å, respectively.

The total energy for the isolated SFC, SFM, SFP, and SFT molecules was computed and fully relaxed in a 20 Å × 20 Å × 20 Å cube box. The electronic energy of these inhibitors was calculated using the same CASTEP-based material studio code as that mentioned above. The partial charges of molecules were calculated from Mulliken analyses. The electronic spin density and overlap atomic matrix were employed to obtain the Mulliken partition charges in the molecule.[68] Furthermore, modeling *Fe*-sulphonamides remains challenging for first-principles periodic calculations because of the large size of the adsorbing systems (e.g., 124 atoms for SFC), which requires significant resources and calculation times.

3. RESULTS AND DISCUSSION

3.1. The Adsorption of Sulphonamides. To better explain the adsorption of sulfonamides on the *Fe* (100) surface, we obtained structural information to construct the final geometries with different initial orientations (unoptimized geometries). Two oxygen atoms are bonded to sulfur atoms in sulphonamides (*O*−*S*−*O*). In this work, we consider two scenarios. In the first scenario, the initial position of the molecules has *O*−*S*−*O* atoms facing toward the surface plane (Figure S1). In the second scenario, the *O*−*S*−*O* atoms face away from the surface (Figure S2). When the initial configuration (unoptimized geometries) *O*−*S*−*O* faces toward the surface, it leads to dissociative adsorption, while *O*−*S*−*O* facing away from the surface leads to molecular adsorption. Juan et al.[69] observed similar characteristics with the adsorption of 2-mercaptoimidazole on the Fe (1 0 0) surface.

3.1.1. Dissociative Adsorption of Sulfacetamide (SFC), Sulfamerazine (SFM), Sulfapyridine (SFP), and Sulfathiazole (SFT). The SFC, SFM, SFP, and SFT dissociation at the *Fe* (100) surface is spontaneous. We only observed this behavior when the initial configuration is directed toward *O*−*S*−*O* atoms facing downward, bonding with the iron atoms and localized at the iron surface. The relaxed structures of these molecules are depicted in Figure 2. The interaction energy and geometrical parameters of the optimized geometries at the Fe (100) surface for the dissociative interaction of the SFC, SFM, SFP, and SFT molecules are listed in Table 1. The geometric orientation of the molecules at the *Fe* (100) surface is described through the tilt angle of the *Z*-axis. The tilt angle of the molecules in the dissociative form is shown in Figure S3. Furthermore, in this study, we understand the modes of bond formation at each location for all forms of sulphonamide molecules and thus is described hereafter.

Table 1. Interaction Energy and Geometrical Parameters of Optimized Geometries at the *Fe* (100) Surface in the Dissociative Form of SFC, SFM, SFP, and SFT Molecules Using the CASTEP Module at the DFT/DFT + D Level[a]

molecule (O−S−O down)	interaction energy DFT (−eV)	interaction energy DFT + D (−eV)	d_{S-Fe} (DFT) (Å)	d_{S-Fe} (DFT + D) (Å)
SFC	3.424	4.680	3.169	3.120
SFM	3.424	4.762	3.049	3.027
SFP	3.476	4.840	3.061	3.029
SFT	2.939	4.235	2.926, 5.878	2.930, 5.869

[a]Where distances of *S* atom from the surface d_{S-Fe} are in Å.

3.1.1.1. Adsorption of the SFC ($C_8H_{10}N_2O_3S$). The first configuration is shown in Figure 2. It relates to SFC in the dissociative form adsorbed by dissociation into (C_2H_4NO) and ($C_6H_6NO_2S$). The dissociation mechanism linked to the formation of an N−Fe bond (of C_2H_4NO) at the top site

https://doi.org/10.1021/acsomega.4c04651
ACS Omega 2024, 9, 38722−38732

and two *O*−*Fe* bonds (of the $C_6H_6NO_2S$) at the *Fe* (100) surface. A similar spontaneous dissociation of 2-mercaptobenzothiazole (MBT) is observed by Chiter et al.,[70] where MBT inhibitors in thione form deprotonated on the surface of *Cu*. The adsorbed molecule makes a bond via *O* atoms and N atoms at a distance of 1.941, 1.943, and 1.933 Å, as shown in Figure 2. The best inhibitors are molecules that strongly bond to iron surfaces. The tilt angle of both fragments of SFC from the surface plane is 61° (Figure S3). The interaction energy of the SFC molecule in dissociative form is −4.680 eV (Table 1) after applying dispersion correction D.

3.1.1.2. Adsorption of the SFM ($C_{11}H_{12}N_4O_2S$). The SFM molecule adsorbed at the Fe (100) surface dissociates into ($C_5H_6N_3$) and ($C_6H_6NO_2S$). The SFM interacts via three covalent bonds on the Fe (100) surface (second snap in Figure 2). This makes bonds via the *O* and *N* atoms to the top site with the bonding *O*−*Fe*, *O*−*Fe*, and *N*−*Fe* at 1.942, 1.949, and 1.965 Å, respectively. In this configuration, we observed that the two O atoms had share between two top sites of the *Fe* atoms. This interaction mode for the SFM at the *Fe* (100) surface well agrees with the interaction of 2-mercaptobenzothiazole (MBT) on the oxidized covered *Cu* surface with an oxide layer, where *S* and *N* make bonds with the *Cu* surface.[71] The adopted orientation is from the aromatic ring containing *S* ($C_6H_6NO_2S$) to the aromatic ring containing *N* atoms ($C_5H_6N_3$) on the Fe surface, and the surface of the molecule is angled about 42° and 90° from the *Fe* surface plane (Figure S3). There is no difference in the interaction energy (−3.424 eV) between SFC and SFM without dispersion correction (Table 1), unveiling that both adsorption types are isoenergetic.

3.1.1.3. Adsorption of SFP ($C_{11}H_{11}N_3O_2S$). The interaction mechanisms and adsorption modes of the SFP are the same as those of SFC and SFM; however, inhibition characteristics are different depending on the locations and bond formation on the surfaces. For SFP, these interaction energies are similar to SFC and SFM of the same orientation on the Fe (100) surface, for which the values were −4.680, −4.762, and −4.840 eV/molecule (Table 1) for SFC, SFM, and SFP, respectively. The adsorbed inhibitors on the Fe (100) must also appear in a geometry that increases the interfacial impedance, thus lowering the current density and general corrosion rate. This issues could be easily handled by the DFT.[31] The maximum interaction energy (−4.840 eV) is found for the SFP in dissociated form at the *Fe* (100) surface. The axis of the SFP molecule for $C_5H_5N_2$ and $C_6H_6NO_2S$ is oriented by 90° and 61°, respectively at the *Fe* (100) plane (Figure S3). Vernack et al.[72] found a similar result for the interaction of MBT at the *Cu* (111) plane. It was discovered that MBT can exhibit strong adsorption in a perpendicular orientation on the Cu (111) surface, bonded via the atom *S* at higher coverage. SFP binds via the *O* and *N* atoms with *O*−*Fe*, *O*−*Fe*, and *N*−*Fe* bond lengths of 1.963, 1.963, and 1.957 Å, respectively (Figure 2).

3.1.1.4. Adsorption of SFT ($C_9H_9N_3O_2S_2$). The *S* atoms of SFT are localized at the distance of 2.930 and 5.869 Å after applying the dispersion correction on the iron surface and not making a bond to *Fe* atoms (fourth snapshot in Figure 2 and Table 1). The *O* atoms of SFT accommodate at top sites through bond lengths of 1.946 and 1.988 Å at the *Fe* (100) surface. The interaction energy of the SFT is −4.235 eV (Table 1) after applying dispersion correction. The weak adsorption of the SFT is attributed to one of the fragments not bonded via the surface (Figure 2). The SFT, too, adsorbed in a perpendicular position like SFP on the *Fe* (100) plane. After the adsorption, tilt angles are 90° and 61° for the fragment $C_3H_3N_2S$ and $C_6H_6NO_2S$, respectively (Figure S3).

The complete dissociation process of the sulphonamides shown in Figure 2 will be treated within the forthcoming work, where the competitive effectiveness, i.e., inhibitors-water, inhibitors-acids, inhibitors-metals, will be theoretically considered as described by others.[33,73,70] Thus, only the molecular adsorption mechanism of sulphonamides is presented hereafter.

3.1.2. Molecular Adsorption of Sulfacetamide (SFC), Sulfamerazine (SFM), Sulfapyridine (SFP), and Sulfathiazole (SFT). It is better to demonstrate the molecular adsorption in the presence of acids and solvents present in the medium described by SEM obtained in the experiment;[74] however, the dissociation of the sulphonamides reflects the stability of the geometries. The interaction energy and the geometrical parameters of the optimized geometries at the *Fe* (100) surface for the SFC, SFM, SFP, and SFT molecules are depicted in Table 2. The negative interaction energy (E_{int}) illustrates the spontaneity of the adsorption phenomenon of inhibiting molecules at the metal surface. The E_{int} for molecular adsorption of the SFC, SFM, SFP, and SFT at the *Fe* (100) surface using DFT functionals are −1.656, −0.642, −0.986, and −2.727 V, respectively. All of the sulfonamide molecules are chemically adsorbed at the *Fe* (100) surface. The previous analysis indicates that a E_{int} less than −20 kJ/mol (−0.207 eV) on mild steel shows that the adsorption mechanism is characterized by a physical nature; and more than −40 kJ/mol (−0.415 eV), it occurs chemically.[75−78] The top and side snaps of relaxed geometries for molecular adsorption of the SFC, SFM, SFP, and SFT molecules at the *Fe* (100) surface are depicted in Figure 3. The bond length of the *Fe*−*O* in the SFC is of the order of 1.906 Å; however, the bonding length of the *Fe*−*N* is found to be 2.228 Å (Figure 3). Thus, the SFC adopted the orientation wherein the *O* atom is closer than the *N* atom on the *Fe* surface. The SFM molecule did not make a bond with the surface wherein the *S* atom sits at 7.012 Å from the surface (Table 2).

Table 2. Interaction Energy and Geometrical Parameters of Optimized Geometries at the *Fe* (100) Surface in the Molecular Form of the SFC, SFM, SFP, and SFT Molecules Using the CASTEP Module at the DFT/DFT + D level[a]

molecule (O−S−O up)	interaction energy DFT (−eV)	interaction energy DFT + D (−eV)	d_{S-Fe} (DFT) (Å)	d_{S-Fe} (*DFT* + *D*) (Å)
SFC	1.656	3.421	4.807	4.796
SFM	0.642	2.329	7.014	7.012
SFP	0.986	2.912	5.881	5.878
SFT	2.727	4.733	5.450, 1.840	5.439, 1.835

[a]Where distances of *S* atom from the surface d_{S-Fe} are in Å.

The SFP adsorbed covalently through *C* atoms at the top site, and the bonding length of *Fe*−*C* is 2.171 Å (Figure 3). The SFT molecule makes a bond via *S* and *N* atoms at 2.301, 2.489, and 2.163 Å, as shown in Figure 3. The total interaction energy difference (ΔE) in Tables 1 and 2 for SFT is 0.498 eV with D; however, the ΔE is only 0.212 eV without D.

For further geometrical information, the side view of the plane for a tilt angle of the SFC, SFM, SFP, and SFT to the iron surface is shown in Figure S4. The SFP and SFT adsorbed

https://doi.org/10.1021/acsomega.4c04651
ACS Omega 2024, 9, 38722−38732

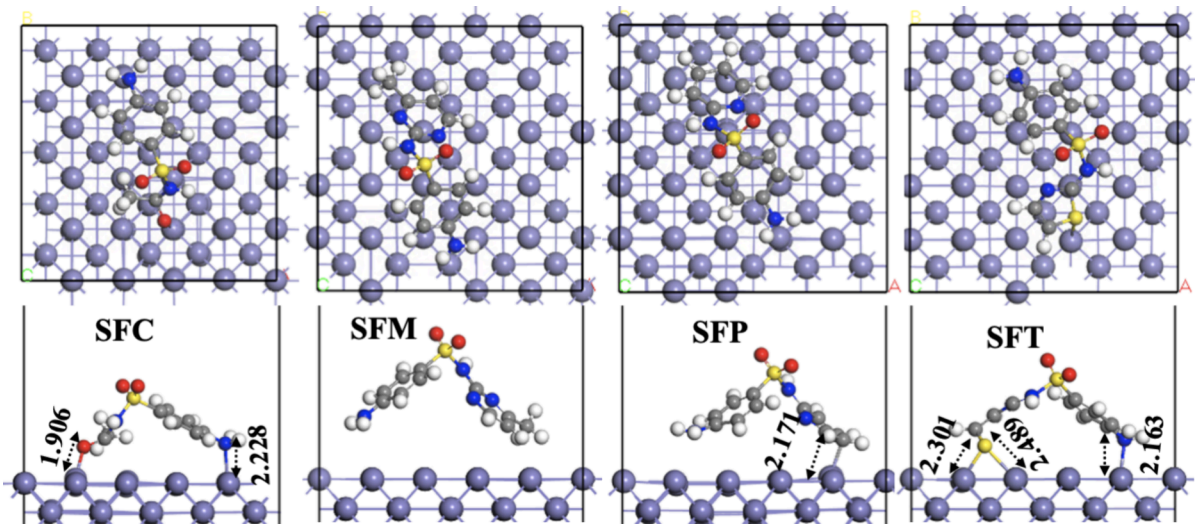

Figure 3. Top and side views for the relaxed structure of the molecular adsorption of the SFC, SFM, SFP, and SFT molecules at the *Fe* (100) surface using the CASTEP module at the DFT + D level. In the neutral molecule, the red is *O* atoms. The yellow is *S* atoms. The light gray is *C* atoms. The dark blue is *N* atoms. The light blue is *Fe* atoms, and the white is *H* atoms. The bond lengths are given in Å.

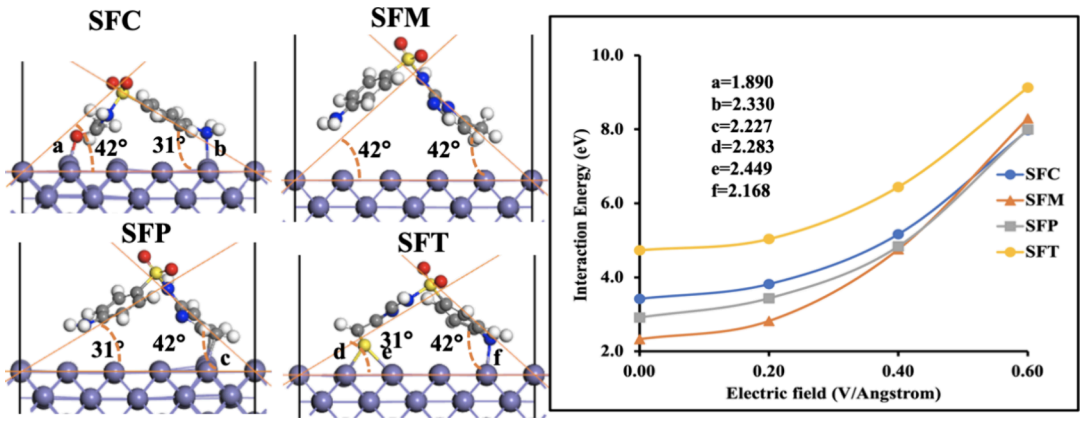

Figure 4. Relaxed geometries (left) of molecular adsorption and (right) variation in the interaction energy for the SFC, SFM, SFP, and SFT molecules at the Fe (100) surface after applying 0.6 eV electric field using the CASTEP module at the DFT + D level. In the neutral molecule, the red is *O* atoms. The yellow is *S* atoms. The light gray is *C* atoms. The dark blue is *N* atoms. The light blue is *Fe* atoms, and the white is *H* atoms. The alphabets a−c in Å are the bonds made with the surface.

at the Fe (100) surface shown in snapshot of Figure S3 make a similar tilt angle from the surfaces. The orientation of the *Z* axis for SFP and SFT is about 31° and 42°, respectively.

3.1.2.1. Molecular Adsorption of Sulfacetamide (SFC), Sulfamerazine (SFM), Sulfapyridine (SFP), and Sulfathiazole (SFT) with an Electric Field. Microbes at the surface influence the corrosion rate; therefore, we applied an electric field on the surface to understand the adsorption mechanism. In our previous work,[45] we described the geometrical and electronic densities of the iron for *H*, *S*, and SO_4 utilizing an electric field for the adsorption on the *Fe* (100) surface. Electric field as a microbe is chosen, on one hand, to avoid complexities and, on the other hand, to avoid finding unavailable/inaccessible structural information on the microbes to consider at the DFT level. The optimized geometries (left) of the molecular adsorption and (right) change in the interaction energy for the SFC, SFM, SFP, and SFT molecules at the *Fe* (100) surface after applying 0−0.6 eV electric field are shown in Figure 4. On the application of an electric field at the slab, the geometries of the interacting molecules are the same as those without electric field. We remind that the SFC plane lies at an angle of about 42°, 31° to the surface, with *O* and N atoms facing toward the surface, which favors covalent bond formation between the inhibitors and the *Fe* (100) surface. The SFP also makes a covalent bonding via the *C* atom on the top site. The *Fe*−*C* bond length is 2.227 Å. Here, the *Z* axis of the SFP is angled 42° with the plane (Figure 4).

The interaction energies for molecular adsorption of the SFC, SFM, SFP, and SFT at the *Fe* (100) surface using DFT + D functionals are −7.972, −8.296, −7.993, and −9.129 eV, respectively, after applying 0.6 eV electric field. This molecular adsorption of sulfonamides resembles dissociative adsorption, and the results obtained on *Fe* (100) surfaces by applying an electric field showed that absolute interaction energy increases with an increase in the electric field.

The interaction energy is dissimilar (presence/absence of electric field), and we can believe that the microbial corrosion inhibition mechanism to vary depends on the sulfonamides' local bonding and interaction competency. The SFT molecules have the highest interaction energy and therefore would be the best microbial inhibition; however, it is extremely difficult to distinguish between normal and microbial corrosion inhibitors

https://doi.org/10.1021/acsomega.4c04651
ACS Omega 2024, 9, 38722−38732

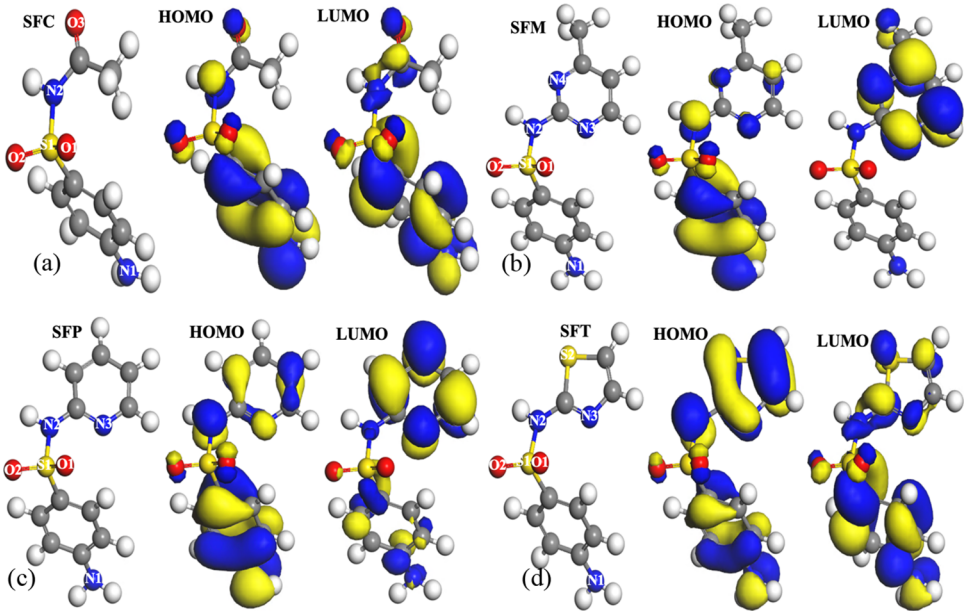

Figure 5. Highest occupied molecular orbital (HOMO) and lowest unoccupied molecular orbital (LUMO) for (a) SFC, (b) SFM, (c) SFP, and (d) SFT using DFT at the DMole3 module. In the neutral molecule, the red is *O* atoms. The yellow is *S* atoms. The light gray is *C* atoms. The dark blue is *N* atoms. The light blue is *Fe* atoms, and the white is *H* atoms. 1, 2, 3, and 4 are the atom indexes.

as both forms of corrosion occur simultaneously. The interaction energy for the SFC, SFP, and SFT agglomerates at a higher electric field (Figure 4, right).

3.2. Electronic Structure Analysis. For further insights into the sulfonamides-Fe contacts, electronic structure analysis of the SFC, SFM, SFP, and SFT is performed, which gives significant information for reactive sites of the sulfonamides and electron transfer with the substrate. We calculated the various electronic descriptors for the sulfonamides and charge analysis. We also plotted the density of states (DOS) for free molecules and the adsorbing system. Furthermore, we calculated the charge density variation ($\Delta\rho$) to confirm the bonding mechanisms.

3.2.1. Electronic Descriptors. It is well-known that frontier molecular orbitals govern the reactivity of sulphonamides. HOMO/LUMO of sulfonamides is linked with the electron donating/accepting capability of the molecule. However, the energy of LUMO shows the capability of the inhibitors/molecule to accept electrons. The lower value of the energy of LUMO, the higher the probability; molecule would take electrons.[31] HOMO and LUMO levels for the optimized geometry of SFC, SFM, and SFT are shown in Figure 5. From all these figures, it is evident that SFC, SFM, SFP, and SFT display electron-rich regions capable of sharing electrons to the *Fe* (100) surface, which enhances their capability to inhibit iron corrosion by establishing a molecule barrier. The quantum chemical descriptors for SFC, SFM, SFP, and SFT are shown in Table 3. Additional information is included in the Supporting Information.

The estimated eigenvalues for HOMO of SFC, SFM, SFP, and SFT molecules are −5.972, −5.547, −5.496, and −5.501 eV, respectively. These low occupied orbitals eigenvalues denote that the electrons needed a little electrons volt of energy to be ionized (i.e., +5.972 and +5.547 eV for SFC and SFM, respectively) and therefore easily shared with the Fe (100) surface. As anticipated, the HOMOs of SFC, SFM, SFP, and SFT are mostly localized on the π-system of the benzene ring (carbonyl group). LUMO for the SFM is concentrated toward aromatic rings having N atoms (Figure 5).

Table 3. Estimated Chemical Descriptors (Quantum) for the SFC, SFM, SFP, and SFT Using the DMole3 Module[a]

molecule	SFC	SFM	SFP	SFT
experimental inhibition efficiency[74]	38.42%	84.56%	76.84%	69.64%
E_{HOMO} (eV)	−5.972	−5.547	−5.496	−5.501
E_{LUMO} (eV)	−1.794	−1.819	−1.562	−1.515
ΔE_G (eV)	4.178	3.728	3.934	3.986
I (eV)	5.972	5.547	5.496	5.501
A (eV)	1.794	1.819	1.562	1.515
χ (eV)	3.883	3.683	3.529	3.508
η (eV)	2.089	1.864	1.967	1.993
σ	0.479	0.536	0.508	0.502
ω	3.609	3.639	3.166	3.087
ω_k^+	5.811	5.713	5.176	5.090
ω_k^-	1.928	2.030	1.647	1.582
$\Delta\omega_k^{\pm}$	7.740	7.743	6.823	6.673
$\Delta E_{back-donation}$	−0.522	−0.466	−0.492	−0.498
ΔN	0.028	0.085	0.120	0.123

[a] I is ionization potential, A is electron affinity, χ is absolute electronegativity, η is global hardness, σ is global softness, ω is global electrophilicity, ω_k^+ is electron accepting powers, ω_k^- is electron donating power, ΔN is fraction of electrons transferred, and $\Delta E_{back-donation}$ is electron back-donation.

Furthermore, the energy gap (ΔE_{gap}) between HOMO and LUMO of sulfonamides is a significant parameter that would be estimated for inhibition of sulphonamides. The lower value of the ΔE_{gap} is linked with enhanced inhibition efficiency of the sulphonamides.[4,79,80] The SFM exhibits the smallest ΔE_{gap}, measured at 3.728 eV, while the SFC demonstrates the highest ΔE_{gap} at 4.178 eV. This observation aligns well with the experimental inhibition efficiency shown in Table 3.

Pearson[81] proposed that in the inhibitors where the HOMO is occupied with electrons, the electronegativity subdivides the

https://doi.org/10.1021/acsomega.4c04651
ACS Omega 2024, 9, 38722−38732

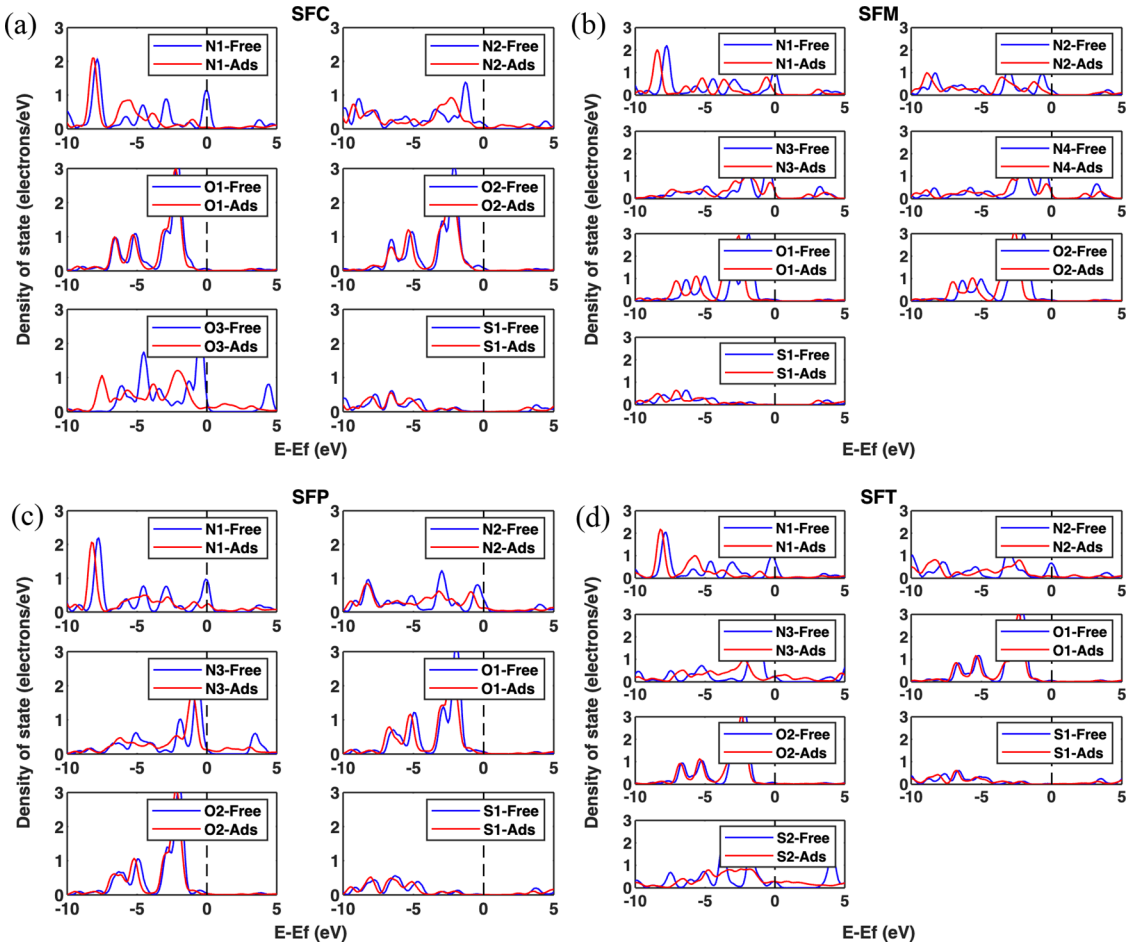

Figure 6. DOS of molecular adsorption for (a) SFC, (b) SFM, (c) SFP, and (d) SFT of various atoms at the *Fe* (100) surface. E_f denotes the Fermi energy level (0 eV). *S*, *N*, and *O* are the heteroatoms of sulphonamides. 1, 2, 3, and 4 are the atom indexes depicted in Figure 5.

ΔE_{gap} into two parts, and the addition of these parts presents the chemical hardness. It is well-known from previous works that global hardness (η) shows the resistance toward the polarization of an electron cloud of atom/ion/molecules.[82] In addition, molecule/inhibitor with a high value of global softness (σ) would easily react and be adsorbed on the iron surface. However, the molecule with a higher global hardness value (lower global softness value) is anticipated to show lower corrosion inhibition efficiency[4] (weak interaction). In the present study, the global hardness of the SFC is the highest (minimum global softness). The global hardness follows the order of SFC > SFT > SFP > SFM, which agrees to experimental inhibition efficiency.[74] The high global softness of 0.479, 0.536, 0.508, and 0.502 (Table 3) for SFC, SFM, SFP, and SFT indicates that they are suitable candidates for robust and efficient adsorption with the *Fe* (100) surface.

The SFM exhibits the smallest $-\Delta E_{back-donation}$, measured at 0.466, while the SFC demonstrates the highest$-\Delta E_{back-donation}$ at 0.522. This observation also aligns well with the experimental inhibition efficiency shown in Table 3. However, Kokalj et al.[83] reported severe doubts about the direct link between the molecular parameter of inhibitors and inhibition efficiency.

Furthermore, the predicted fractions of electrons (ΔN) transferred of the SFC, SFM, SFP and SFT are 0.028, 0.085, 0.120, and 0.123, respectively, showing the tendency of these inhibitors to mutually share electrons at the Fe (100) surface.

3.2.2. Population Analysis. Mulliken established an intuitive method of subdividing molecules into atoms and providing a combined treatment of the covalent bonds and extreme ionic limits at a reasonable computational cost.[84] It is commonly known that the numeric value of Mulliken electronic charges on the atoms has little/no implication; however, relative values of charges are meaningful.[85] A negative value implies antibonding, while a positive value implies a bonding state. The *N1* and *N2* atoms of the SFC gain a charge of 0.1 e^- and 0.06 e^-, respectively, after the adsorption (comparing free state and adsorbed state) at the *Fe* (100) surface. The Mulliken negative charge of the SFM for the atoms *N1, N2, N3*, and *N4* before the adsorption was 0.88, 0.82, 0.45, and 0.45 e^-, respectively; however, they become 0.73, 0.82, 0.35, and 0.38 e^-, respectively, after the adsorption. The *O* atoms of the sulphonamides (SFC, SFM, SFP, and SFT) also gain a little Mulliken charge after the adsorption at the *Fe* (100) surface. Alamiery et al.[86] successfully used the Mulliken analysis for theoretical study with adsorption of thiosemicarbazide for determining the inhibition adsorption site. They found that increased electronegativity around heteroatoms (*S*, *N*, and *O*) favors the adsorption. A significant change in the charges (0.28 e^- to 0.03 e^-) occurs for the *S2* atom of the SFT molecule.

3.2.3. Electron Density. The DOS for sulphonamides demonstrates the spreading of electrons on the energy scale which is crucial to electrical conductivity[87] of the components

https://doi.org/10.1021/acsomega.4c04651
ACS Omega 2024, 9, 38722−38732

Table 4. Atomic Charges (Mulliken) for the Molecular Adsorption of SFC, SFM, SFP, and SFT of Various Atoms at the Fe (100) Surface[a]

	free state									adsorbed state								
	N1	*N2*	*N3*	*N4*	*O1*	*O2*	*O3*	*S1*	*S2*	*N1*	*N2*	*N3*	*N4*	*O1*	*O2*	*O3*	*S1*	*S2*
molecule		($-e^-$)				($-e^-$)		(e^-)			($-e^-$)				($-e^-$)		(e^-)	
SFC	0.88	0.85			0.91	0.91	0.55	2.15		0.78	0.79			0.90	0.91	0.53	2.13	
SFM	0.88	0.82	0.45	0.45	0.90	0.93		2.15		0.73	0.82	0.35	0.38	0.88	0.92		2.16	
SFP	0.88	0.82	0.43		0.90	0.93		2.15		0.74	0.78	0.42		0.88	0.92		2.14	
SFT	0.88	0.81	0.42		0.88	0.93		2.15	0.28	0.76	0.81	0.38		0.88	0.91		2.13	0.03

[a] *S*, *N*, and *O* are the heteroatoms of sulphonamides. 1, 2, 3, and 4 are the atom indexes depicted in Figure 5.

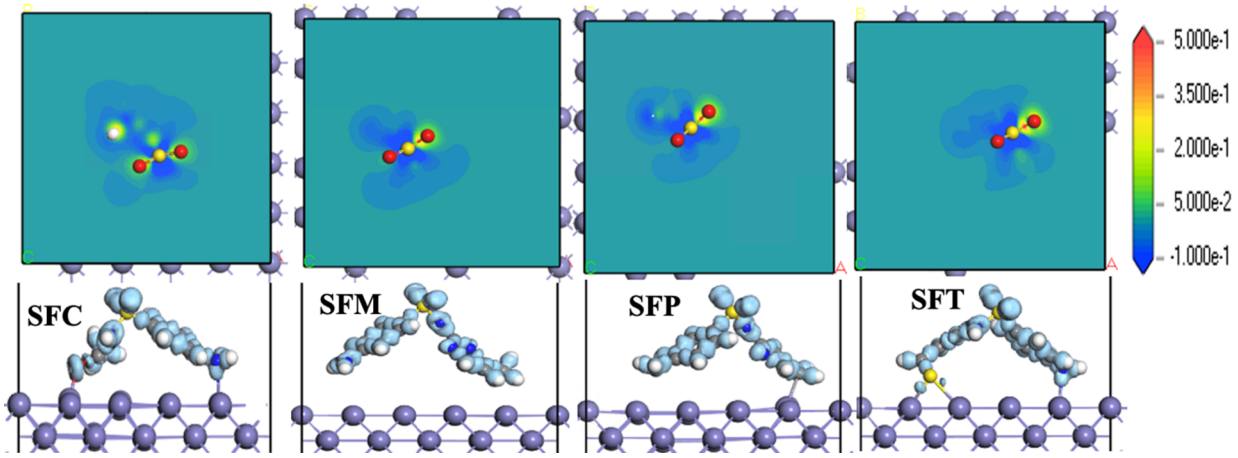

Figure 7. $\Delta\rho$ (side view) for molecular adsorption of SFC, SFM, SFP, and SFT at the *Fe* (100) surfaces. A slice is sketched through sulfur atom S1 and depicted as a top view. At the scale (right), the blue section indicates charge depletion, and the red section indicates charge accumulation.

in the corrosive (electrochemical) environment. For fundamental understanding of inhibition, the DOS of sulfonamides in the adsorbed state is compared with the isolated (free) state. The DOS of the SFC, SFM, SFP, and SFT molecules for the heteroatoms (*S, N, O*) is shown in Figure 6. The zero value on the energy scale is the Fermi energy level. The first peak in free state of nitrogen atoms *N1* and *N2* for the SFC occurs near zero and −1.30 eV, respectively; however, it shifted to −1.09and −2.20 eV after adsorption on the energy scale. The DOS of the *S1* atom in sulphonamides (SFC, SFM, SFP, andSFT) experiences a minor shift, while the *S2* atom in the SFT undergoes a significant change. A similar finding is observed in the Mulliken charge analysis detailed in Table 4, showcasing an alteration of around 0.02eV for *S1* and a 0.25 eV change for *S2* atom. The shift of the DOS toward a low energy level for the SFC, SFM, SFP, and SFT atoms implies the stabilization of sulphonamides at the Fe (100) surface. The energy shift in atomic orbitals is alike to the alkanethiol molecule adsorbed at the iron surface.[88] The first peak of oxygen atoms *O1* and *O2* for the SFM shifted by 0.73 and 0.61 eV, respectively, toward lower energy on the DOS scale. Jibiao et al.[89] demonstrated that the *Fe* (100) valence band had a key role in the adsorbate-*Fe* interaction.

3.2.4. Electron Density Difference. To get further details for the charge distribution of inhibitors, electron density difference ($\Delta\rho$) is computed at an iso-surface of $\pm 0.1 \frac{e^-}{Å^3}$ for sulfonamides. The $\Delta\rho$ value is estimated using eq 3.

$$\Delta\rho = \rho_{\text{ironslab}/x} - (\rho_{\text{ironslab}} + \rho_x) \quad (3)$$

where x corresponds to inhibiting species such as SFC, SFM, SFP, and SFT molecules, $\rho_{\text{ironslab}/x}$ is the electron density (ED) of the *Fe* slab with inhibiting species x, ρ_{ironslab} is the ED of the clean surface of the *Fe* slab, and ρ_x is the ED of species x in a free state. The $\Delta\rho$ for molecular adsorption of SFC, SFM, SFP, and SFT at the *Fe* (100) surfaces is shown in Figure 7. A significant change in the charges around the adsorbing sulfonamides demonstrates strong inhibition of these molecules at the *Fe* (100) surface (Figure 7).

Furthermore, a clear depiction can be drawn from the slice sketched parallel to the surface, as shown in the top view of Figure 7. In such a map, electron-poor sites are designated with blue on the scale, electron-rich sites are red-colored, and sites with yellow show moderate charge density. For the inhibitors contacting the *Fe* (100) surface and suppressing corrosion reaction, there is an electron-deficient area more than electron-rich ones for inhibitors on the adsorbing surface (the situation is reversed for the Fe slab). The drawn surfaces shown in Figure 7 indicate that the distribution of colors leads to blue > yellow> red. The maps of SFC and SFT are portrayed by electron-deficient regions much more (broader blue area) than those of SFM and SFP. This agrees with the interaction energy order of SFM < SFP < SFC < SFT. The yellow regions are concentrated around the oxygen atoms, which agrees with the order of the electron density difference (side view in Figure 7) on the *Fe* surface.

4. CONCLUSIONS

The adsorption of the four corrosion inhibitors, SFC, SFM, SFP, and SFT, was performed using DFT. The DFT-based quantum calculations provide a greener pathway for understanding the complexity of microbial corrosion without discharging any environmentally harmful chemicals. The electric field (novel approach) in the *z*-direction is applied to

https://doi.org/10.1021/acsomega.4c04651
ACS Omega 2024, 9, 38722−38732

understand the inhibition effectiveness of these molecules from microbial corrosion at the Fe (100) surface. Associated with the corrosion inhibitor molecules, these results explain the substantially improved inhibition efficacy against the MIC. The interaction energy in the absence of electric field for the molecular adsorption utilizing the DFT + D functional of the SFC, SFM, SFP, and SFT at the Fe (100) surface is −3.421, −2.329, −2.912, and −4.733 eV, respectively. It becomes −7.972, −8.296, −7.993, and −9.129 eV, respectively, after applying 0.6 eV of an electric field. The exceptional increase in the interaction energy of inhibitors at the *Fe* surface and models studied confirmed the reliability of the inhibition effectiveness from the microbes. A comparison of the inhibition efficiency of SFC, SFM, SFP, and SFT studied in this work suggests that their inhibition effect is closely linked to electronic descriptors such as HOMO, LUMO, ionization potential, absolute electronegativity, global softness, global electrophilicity, fraction of electrons transferred, and electron back-donation. The global softness follows the order of SFC < SFT < SFP < SFM, which agrees with the experimental inhibition efficiency. The downward shift (lower energy) in the density of states for the SFC, SFM, SFP, and SFT atoms indicates that these species are stabilized at the *Fe* surface. This is also confirmed by electron density difference maps of the SFC, SFM, SFP, and SFT, which are illustrated by electron-deficient regions much more (broader blue area) than those of electron abundance regions (red area). Furthermore, the negative sign of the interaction energy, HOMO values, and other thermodynamic parameters calculated suggest that the adsorption mechanism is chemisorption.

Investigating the interaction of sulfonamide at an atomistic scale, particularly the mechanism of bond formation, helps understand the protection from initiating localized corrosion.

■ ASSOCIATED CONTENT

Supporting Information

The Supporting Information is available free of charge at https://pubs.acs.org/doi/10.1021/acsomega.4c04651.

Definitions for electronic descriptors and geometric parameter for molecular adsorption (PDF)

■ AUTHOR INFORMATION

Corresponding Author

Faisal Khan − *Mary Kay O'Connor Process Safety Center (MKOPSC), Artie McFerrin Department of Chemical Engineering, Texas A&M University, College Station, Texas 77843-3122, United States;* orcid.org/0000-0002-5638-4299; Email: fikhan@tamu.edu

Authors

Mohammad Asif − *Centre for Risk, Integrity, and Safety Engineering (C-RISE), Faculty of Engineering and Applied Science, Memorial University of Newfoundland, St. John's, NL A1B 3X5, Canada*

N.V. Saidileep Korlapati − *Mary Kay O'Connor Process Safety Center (MKOPSC), Artie McFerrin Department of Chemical Engineering, Texas A&M University, College Station, Texas 77843-3122, United States*

Kelly Hawboldt − *Centre for Risk, Integrity, and Safety Engineering (C-RISE), Faculty of Engineering and Applied Science, Memorial University of Newfoundland, St. John's, NL A1B 3X5, Canada*

Susan Caines − *Centre for Risk, Integrity, and Safety Engineering (C-RISE), Faculty of Engineering and Applied Science, Memorial University of Newfoundland, St. John's, NL A1B 3X5, Canada*

Complete contact information is available at: https://pubs.acs.org/10.1021/acsomega.4c04651

Notes

The authors declare no competing financial interest.

■ ACKNOWLEDGMENTS

M.A. is thankful for financial support provided through Genome Canada and Memorial University, Canada. N.V.S.K. is thankful for the financial support as a Graduate Assistantship from Mary Kay O'Connor Process Safety Center (MKOPSC) at Texas A&M University.

■ REFERENCES

(1) Malik, M. A.; Hashim, M. A.; Nabi, F.; AL-Thabaiti, S. A.; Khan, Z. Anti-corrosion ability of surfactants: A review. *Int. J. Electrochem Sci.* **2011**, *6* (6), 1927−1948.

(2) El-Maksoud, S. A. A. The effect of organic compounds on the electrochemical behaviour of steel in acidic media. *A review. Int. J. Electrochem Sci.* **2008**, *3* (5), 528−555.

(3) Al-Amiery, A. A.; Binti Kassim, F. A.; Kadhum, A. A. H.; Mohamad, A. B. Synthesis and characterization of a novel eco-friendly corrosion inhibition for mild steel in 1 M hydrochloric acid. *Sci. Rep.* **2016**, *6*, 19890.

(4) Kumar, D.; Jain, V.; Rai, B. Unravelling the mechanisms of corrosion inhibition of iron by henna extract: A density functional theory study. *Corros. Sci.* **2018**, *142*, 102−109.

(5) Khaled, K. F. Corrosion control of copper in nitric acid solutions using some amino acids - A combined experimental and theoretical study. *Corros. Sci.* **2010**, *52* (10), 3225−3234.

(6) Ebenso, E. E.; Arslan, T.; Kandemirlı, F.; Love, I.; Öğretır, C.; Saracoğlu, M.; Umoren, S. A. Theoretical studies of some sulphonamides as corrosion inhibitors for mild steel in acidic medium. *Int. J. Quantum Chem.* **2010**, *110* (14), 2614−2636.

(7) Solomon, M. M.; Umoren, S. A.; Udosoro, I. I.; Udoh, A. P. Inhibitive and adsorption behaviour of carboxymethyl cellulose on mild steel corrosion in sulphuric acid solution. *Corros. Sci.* **2010**, *52* (4), 1317−1325.

(8) Bayol, E.; Gürten, A. A.; Dursun, M.; Kayakirilmaz, K. Adsorption behavior and inhibition corrosion effect of sodium carboxymethyl cellulose on mild steel in acidic medium. *Wuli Huaxue Xuebao/ Acta Phys. - Chim Sin.* **2008**, *24* (12), 2236−2243.

(9) Khairou, K. S.; El-Sayed, A. Inhibition effect of some polymers on the corrosion of cadmium in a hydrochloric acid solution. *J. Appl. Polym. Sci.* **2003**, *88* (4), 866−871.

(10) Umoren, S. A.; Obot, I. B.; Ebenso, E. E.; Okafor, P. C.; Ogbobe, O.; Oguzie, E. E. Gum arabic as a potential corrosion inhibitor for aluminium in alkaline medium and its adsorption characteristics. *Anti-Corrosion Methods Mater.* **2006**, *53* (5), 277−282.

(11) Hassan, R. M.; Zaafarany, I. A. Kinetics of corrosion inhibition of aluminum in acidic media by water-soluble natural polymeric pectates as anionic polyelectrolyte inhibitors. *Materials (Basel).* **2013**, *6* (6), 2436−2451.

(12) El-Haddad, M. N. Chitosan as a green inhibitor for copper corrosion in acidic medium. *Int. J. Biol. Macromol.* **2013**, *55*, 142−149.

(13) Abdel-Gaber, A. M.; Hijazi, K. M.; Younes, G. O.; Nsouli, B. Comparative study of the inhibitive action between the bitter orange leaf extract and its chemical constituent linalool on the mild steel corrosion in HCL solution. *Quim Nova.* **2017**, *40* (4), 395.

(14) Rajeswari, V.; Kesavan, D.; Gopiraman, M.; Viswanathamurthi, P. Physicochemical studies of glucose, gellan gum, and hydroxypropyl cellulose - Inhibition of cast iron corrosion. *Carbohydr. Polym.* **2013**, *95* (1), 288−294.

(15) Bentrah, H.; Rahali, Y.; Chala, A. Gum Arabic as an eco-friendly inhibitor for API 5L X42 pipeline steel in HCl medium. *Corros. Sci.* **2014**, *82*, 426−431.
(16) Li, H.; Zhang, Y.; Li, C.; Zhou, Z.; Nie, X.; Chen, Y.; Cao, H.; Liu, B.; Zhang, N.; Said, Z.; Debnath, S. Cutting fluid corrosion inhibitors from inorganic to organic: Progress and applications. *Korean J. Chem. Eng.* **2022**, *39* (5), 1107−1134.
(17) Salleh, S. Z.; Yusoff, A. H.; Zakaria, S. K.; Taib, M. A. A.; Seman, A. A.; Masri, M. N.; Mohamad, M.; Mamat, S.; Sobri, S. A.; Ali, A.; Ter Teo, P. Plant extracts as green corrosion inhibitor for ferrous metal alloys: A review. *J. Clean Prod.* **2021**, *304*, No. 127030.
(18) Chaubey, N.; Qurashi, A.; Chauhan, D. S.; Quraishi, M. A. Frontiers and advances in green and sustainable inhibitors for corrosion applications: A critical review. *J. Mol. Liq.* **2021**, *321*, No. 114385.
(19) Singh, A.; Ansari, K. R.; Chauhan, D. S.; Quraishi, M. A.; Lgaz, H.; Chung, I. M. Comprehensive investigation of steel corrosion inhibition at macro/micro level by ecofriendly green corrosion inhibitor in 15% HCl medium. *J. Colloid Interface Sci.* **2020**, *560*, 225−236.
(20) Li, M.; Xu, J.; Li, R.; Wang, D.; Li, T.; Yuan, M.; Wang, J. Simple preparation of aminothiourea-modified chitosan as corrosion inhibitor and heavy metal ion adsorbent. *J. Colloid Interface Sci.* **2014**, *417*, 131−136.
(21) Bello, M.; Ochoa, N.; Balsamo, V.; López-Carrasquero, F.; Coll, S.; Monsalve, A.; González, G. Modified cassava starches as corrosion inhibitors of carbon steel: An electrochemical and morphological approach. *Carbohydr. Polym.* **2010**, *82* (3), 561−568.
(22) Mobin, M.; Khan, M. A.; Parveen, M. Inhibition of mild steel corrosion in acidic medium using starch and surfactants additives. *J. Appl. Polym. Sci.* **2011**, *121* (3), 1558−1565.
(23) Abdallah, M. Guar Gum as Corrosion Inhibitor for Carbon Steel in Sulfuric Acid Solutions. *Port Electrochim Acta.* **2004**, *22* (2), 161−175.
(24) Gowri, S.; Sathiyabama, J.; Rajendran, S. Corrosion inhibition effect of carbon steel in sea water by L-Arginine-Zn2+ system. *Int. J. Chem. Eng.* **2014**.
(25) Chakravarthy, M. P.; Mohana, K. N. Adsorption and Corrosion Inhibition Characteristics of Some Nicotinamide Derivatives on Mild Steel in Hydrochloric Acid Solution. *ISRN Corros* **2014**.
(26) Singh, P.; Srivastava, V.; Quraishi, M. A. Novel quinoline derivatives as green corrosion inhibitors for mild steel in acidic medium: Electrochemical, SEM, AFM, and XPS studies. *J. Mol. Liq.* **2016**, *216*, 164−173.
(27) Cabrini, M.; Lorenzi, S.; Pastore, T. Cyclic voltammetry evaluation of inhibitors for localised corrosion in alkaline solutions. *Electrochim. Acta* **2014**, *124*, 156−164.
(28) Focke, W. W.; Nhlapo, N. S.; Vuorinen, E. Thermal analysis and FTIR studies of volatile corrosion inhibitor model systems. *Corros. Sci.* **2013**, *77*, 88−96.
(29) Hassannejad, H.; Nouri, A. Sunflower seed hull extract as a novel green corrosion inhibitor for mild steel in HCl solution. *J. Mol. Liq.* **2018**, *254*, 377−382.
(30) Guo, L.; Kaya, S.; Obot, I. B.; Zheng, X.; Qiang, Y. Toward understanding the anticorrosive mechanism of some thiourea derivatives for carbon steel corrosion: A combined DFT and molecular dynamics investigation. *J. Colloid Interface Sci.* **2017**, *506*, 478−485.
(31) Obot, I. B.; Macdonald, D. D.; Gasem, Z. M. Density functional theory (DFT) as a powerful tool for designing new organic corrosion inhibitors: Part 1: An overview. *Corros. Sci.* **2015**, *99*, 1−30.
(32) Gece, G. The use of quantum chemical methods in corrosion inhibitor studies. *Corros. Sci.* **2008**, *50* (11), 2981−2992.
(33) Chen, X.; Chen, Y.; Cui, J.; Li, Y.; Liang, Y.; Cao, G. Molecular dynamics simulation and DFT calculation of "green" scale and corrosion inhibitor. *Comput. Mater. Sci.* **2021**, *188*, No. 110229.
(34) Liu, P.; Dai, S.; Lan, J.; Lu, H.; Wang, B.; Zhu, Y. Corrosion inhibition mechanism of imidazole ionic liquids with high temperature in 20% HCl solution. *J. Mol. Model.* **2023**, *29* (1), 29.
(35) Shahini, M. H.; Keramatinia, M.; Ramezanzadeh, M.; Ramezanzadeh, B.; Bahlakeh, G. Combined atomic-scale/DFT-theoretical simulations & electrochemical assessments of the chamomile flower extract as a green corrosion inhibitor for mild steel in HCl solution. *J. Mol. Liq.* **2021**, *342*, No. 117570.
(36) Saraswat, V.; Yadav, M.; Obot, I. B. Investigations on eco-friendly corrosion inhibitors for mild steel in acid environment: Electrochemical, DFT and Monte Carlo Simulation approach. *Colloids Surfaces A Physicochem Eng. Asp.* **2020**, *599*, No. 124881.
(37) Zinad, D. S.; Hanoon, M.; Salim, R. D.; Ibrahim, S. I.; Al-Amiery, A. A.; Takriff, M. S.; Kadhum, A. A. H. A new synthesized coumarin-derived schiff base as a corrosion inhibitor of mild steel surface in hcl medium: Gravimetric and dft studies. *Int. J. Corros Scale Inhib.* **2020**, *9* (1), 228−243.
(38) Madkour, L. H.; Kaya, S.; Guo, L.; Kaya, C. Quantum chemical calculations, molecular dynamic (MD) simulations and experimental studies of using some azo dyes as corrosion inhibitors for iron. Part 2: Bis−azo dye derivatives. *J. Mol. Struct.* **2018**, *1163*, 397−417.
(39) Saha, S. K.; Murmu, M.; Murmu, N. C.; Banerjee, P. Evaluating electronic structure of quinazolinone and pyrimidinone molecules for its corrosion inhibition effectiveness on target specific mild steel in the acidic medium: A combined DFT and MD simulation study. *J. Mol. Liq.* **2016**, *224*, 629−638.
(40) Gu, T.; Xu, D.; Zhang, P.; Li, Y.; Lindenberger, A. L. *Microbiologically influenced corrosion and its impact on metals and other materials*. In Microbiology for Minerals, Metals, Materials and the Environment, 2015.
(41) Rajasekar, A.; Ting, Y. P. Microbial corrosion of aluminum 2024 aeronautical alloy by hydrocarbon degrading bacteria bacillus cereus ACE4 and serratia marcescens ACE2. *Ind. Eng. Chem. Res.* **2010**, *49* (13), 6054−6061.
(42) Zhou, E.; Lekbach, Y.; Gu, T.; Xu, D. Bioenergetics and extracellular electron transfer in microbial fuel cells and microbial corrosion. *Curr. Opin Electrochem.* **2022**, *31*, No. 100830.
(43) Yang, H.; Gong, L.; Wang, H.; Dong, C.; Wang, J.; Qi, K.; Liu, H.; Guo, X.; Xia, B. Y. Preparation of nickel-iron hydroxides by microorganism corrosion for efficient oxygen evolution. *Nat. Commun.* **2020**, *11* (1), 5075.
(44) Oguzie, E. E.; Oguzie, K. L.; Akalezi, C. O.; Udeze, I. O.; Ogbulie, J. N.; Njoku, V. O. Natural products for materials protection: Corrosion and microbial growth inhibition using Capsicum frutescens biomass extracts. *ACS Sustain Chem. Eng.* **2013**, *1* (2), 214−225.
(45) Asif, M.; Khan, F.; Hawboldt, K. Atomistic Analysis of the Microbial Influence on the Adsorption Characteristic of Sulfur, Hydrogen, and SO4 on Iron Surfaces. *Ind. Eng. Chem. Res.* **2023**, *62* (48), 20777−20788.
(46) Little, B. J.; Blackwood, D. J.; Hinks, J.; Lauro, F. M.; Marsili, E.; Okamoto, A.; Rice, S. A.; Wade, S. A.; Flemming, H. C. Microbially influenced corrosion—Any progress? *Corros. Sci.* **2020**, *170*, No. 108641.
(47) Arslan, T.; Kandemirli, F.; Ebenso, E. E.; Love, I.; Alemu, H. Quantum chemical studies on the corrosion inhibition of some sulphonamides on mild steel in acidic medium. *Corros. Sci.* **2009**, *51* (1), 35−47.
(48) Fang, J.; Li, J. Quantum chemistry study on the relationship between molecular structure and corrosion inhibition efficiency of amides. *J. Mol. Struct Theochem.* **2002**, *593* (1−3), 179.
(49) Zhao, P.; Liang, Q.; Li, Y. Electrochemical, SEM/EDS and quantum chemical study of phthalocyanines as corrosion inhibitors for mild steel in 1 mol/L HCl. *Appl. Surf. Sci.* **2005**, *252* (5), 1596−1607.
(50) Abuelela, A. M.; Kaur, J.; Saxena, A.; Bedair, M. A.; Verma, D. K.; Berdimurodov, E. Electrochemical and DFT studies of Terminalia bellerica fruit extract as an eco-friendly inhibitor for the corrosion of steel. *Sci. Rep.* **2023**, *13* (1), 1−22.
(51) Badr, E. A.; Bedair, M. A.; Shaban, S. M. Adsorption and performance assessment of some imine derivatives as mild steel corrosion inhibitors in 1.0 M HCl solution by chemical, electro-

https://doi.org/10.1021/acsomega.4c04651
ACS Omega 2024, 9, 38722−38732

chemical and computational methods. *Mater. Chem. Phys.* **2018**, *219*, 444−460.
(52) Kohn, W. Nobel lecture: Electronic structure of matter - Wave functions and density functional. *Rev. Mod. Phys.* **1999**, *71* (5), 1253.
(53) Burke, K. Perspective on density functional theory. *J. Chem. Phys.* **2012**, *136* (15), No. 150901.
(54) Becke, A. D. Perspective: Fifty years of density-functional theory in chemical physics. *J. Chem. Phys.* **2014**, *140* (18), No. 18A301.
(55) Yu, H. S.; Li, S. L.; Truhlar, D. G. Perspective: Kohn-Sham density functional theory descending a staircase. *J. Chem. Phys.* **2016**, *145* (13), No. 130901.
(56) Perdew, J. P.; Burke, K.; Ernzerhof, M. Generalized Gradient Approximation Made Simple. *Phys. Rev. Lett.* **1997**, *78*, 1396.
(57) Delley, B. *An all-electron numerical method for solving the local density functional for polyatomic molecules* **1990**, *92*, 508−517.
(58) Segall, M. D.; Lindan, P. J.; Probert, M. A.; Pickard, C. J.; Hasnip, P. J.; Clark, S. J.; Payne, M. C. First-principles simulation: Ideas, illustrations and the CASTEP code. *J. Phys.: Condens. Matter* **2002**, *14* (11), 2717.
(59) Henry, D. J.; Varano, A.; Yarovsky, I. Performance of numerical basis set DFT for aluminum clusters. *J. Phys. Chem. A* **2008**, *112* (40), 9835−9844.
(60) Zhou, Q.; Su, X.; Ju, W.; Yong, Y.; Li, X.; Fu, Z.; Wang, C. Adsorption of H 2 S on graphane decorated with Fe, Co and Cu: a DFT study. *RSC advances.* **2017**, *7* (50), 31457−31465.
(61) Inada, Y.; Orita, H. Efficiency of numerical basis sets for predicting the binding energies of hydrogen bonded complexes: Evidence of small basis set superposition error compared to Gaussian basis sets. *J. Comput. Chem.* **2008**, *29* (2), 225−232.
(62) Asif, M.; Khan, F.; Hawboldt, K.; Anwar, S. Sulfide (H2S) Corrosion Modeling of Cr-Doped Iron (Fe) Using a Molecular Modeling Approach. *ACS Omega.* **2023**, *8* (8), 7395−7406.
(63) Liu, S.; Li, Y. W.; Wang, J.; Jiao, H. Reaction of CO, H2O, H2 and CO2 on the clean as well as O, OH and H precovered Fe(100) and Fe(111) surfaces. *Catal. Sci. Technol.* **2017**, *7* (2), 427−440.
(64) Liu, S.; Tian, X.; Wang, T.; Wen, X.; Li, Y. W.; Wang, J.; Jiao, H. High Coverage Water Aggregation and Dissociation on Fe(100): A Computational Analysis. *J. Phys. Chem. C* **2014**, *118* (45), 26139−26154.
(65) Monkhorst, H. J.; Pack, J. D. Special points for Brillouin-zone integrations. *Phys. Rev. B* **1976**, *13*, 5188.
(66) Kittel, C. *Introduction to Solid State Physics*, 8th ed. Wiley Sons: New York, NY, 2004.
(67) Kumar, D.; Jain, V.; Rai, B. Imidazole derivatives as corrosion inhibitors for copper: A DFT and reactive force field study. *Corros. Sci.* **2020**, *171*, No. 108724.
(68) Clark, S. J.; Segall, M. D.; Pickard, C. J.; Hasnip, P. J.; Probert, M. I.; Refson, K.; Payne, M. C. First principles methods using CASTEP. *Z. Kristallogr.* **2005**, *220*, 567−570.
(69) Radilla, J.; Negrón-Silva, G. E.; Palomar-Pardavé, M.; Romero-Romo, M.; Galván, M. DFT study of the adsorption of the corrosion inhibitor 2-mercaptoimidazole onto Fe(1 0 0) surface. *Electrochim. Acta* **2013**, *112*, 577−586.
(70) Chiter, F.; Costa, D.; Maurice, V.; Marcus, P. Corrosion inhibition of locally de-passivated surfaces by DFT study of 2-mercaptobenzothiazole on copper. *npj Mater. Degrad.* **2021**, *5* (1), 2410.
(71) Chiter, F.; Costa, D.; Maurice, V.; Marcus, P. DFT investigation of 2-mercaptobenzothiazole adsorption on model oxidized copper surfaces and relationship with corrosion inhibition. *Appl. Surf. Sci.* **2021**, *537*, No. 147802.
(72) Vernack, E.; Costa, D.; Tingaut, P.; Marcus, P. DFT studies of 2-mercaptobenzothiazole and 2-mercaptobenzimidazole as corrosion inhibitors for copper. *Corros. Sci.* **2020**, *174*, No. 108840.
(73) Hamdan, A. B.; Haider, F. I. Study on tea leaves extract as green corrosion inhibitor of mild steel in hydrochloric acid solution. *IOP Conf. Ser.: Mater. Sci. Eng.* **2018**, *290*, No. 012086.
(74) Obayes, H. R.; Al-Amiery, A. A.; Alwan, G. H.; Abdullah, T. A.; Kadhum, A. A. H.; Mohamad, A. B. Sulphonamides as corrosion inhibitor: Experimental and DFT studies. *J. Mol. Struct.* **2017**, *1138*, 27−34.
(75) Verma, D. K.; Kazi, M.; Alqahtani, M. S.; Syed, R.; Berdimurodov, E.; Kaya, S.; Salim, R.; Asatkar, A.; Haldhar, R. N−hydroxybenzothioamide derivatives as green and efficient corrosion inhibitors for mild steel: Experimental, DFT and MC simulation approach. *J. Mol. Struct.* **2021**, *1241*, No. 130648.
(76) Verma, C.; Quraishi, M. A.; Ebenso, E. E.; Obot, I. B.; El Assyry, A. 3-Amino alkylated indoles as corrosion inhibitors for mild steel in 1M HCl: Experimental and theoretical studies. *J. Mol. Liq.* **2016**, *219*, 647−660.
(77) Verma, D. K.; Khan, F.; Bahadur, I.; Salman, M.; Quraishi, M. A.; Verma, C.; Ebenso, E. E. Inhibition performance of Glycine max, Cuscuta reflexa and Spirogyra extracts for mild steel dissolution in acidic medium: Density functional theory and experimental studies. *Results Phys.* **2018**, *10*, 665−674.
(78) Berdimurodov, E.; Kholikov, A.; Akbarov, K.; Guo, L.; Abdullah, A. M.; Elik, M. A gossypol derivative as an efficient corrosion inhibitor for St2 steel in 1 M HCl + 1 M KCl: An experimental and theoretical investigation. *J. Mol. Liq.* **2021**, *328*, No. 115475.
(79) Karzazi, Y.; Mohammed, M. E. A.; Dafali, A.; Hammouti, B. A theoretical investigation on the corrosion inhibition of mild steel by piperidine derivatives in hydrochloric acid solution. *J. Chem. Pharm. Res.* **2014**, *6* (4), 689−696.
(80) Ahamad, I.; Prasad, R.; Quraishi, M. A. Thermodynamic, electrochemical and quantum chemical investigation of some Schiff bases as corrosion inhibitors for mild steel in hydrochloric acid solutions. *Corros. Sci.* **2010**, *52* (3), 933−942.
(81) Pearson, R. G. Chemical hardness and density functional theory. *J. Chem. Sci.* **2005**, *117* (5), 369.
(82) Kathirvel, K.; Thirumalairaj, B.; Jaganathan, M. Quantum Chemical Studies on the Corrosion Inhibition of Mild Steel by Piperidin-4-One Derivatives in 1 M H3PO4. *Open J. Met.* **2014**, *4* (4), 73.
(83) Kokalj, A.; Lozinšek, M.; Kapun, B.; Taheri, P.; Neupane, S.; Losada-Pérez, P.; Xie, C.; Stavber, S.; Crespo, D.; Renner, F. U.; Mol, A. Simplistic correlations between molecular electronic properties and inhibition efficiencies: Do they really exist? *Corros. Sci.* **2021**, *179*, No. 108856.
(84) Reed, A. E.; Weinstock, R. B.; Weinhold, F. Natural population analysis. *J. Chem. Phys.* **1985**, *83* (2), 735−746.
(85) Segall, M.; Shah, R.; Pickard, C.; Payne, M. Population analysis of plane-wave electronic structure calculations of bulk materials. *Phys. Rev. B - Condens Matter Mater. Phys.* **1996**, *54*, 16317.
(86) Alamiery, A. A.; Isahak, W. N. R. W.; Takriff, M. S. Inhibition of mild steel corrosion by 4-benzyl-1-(4-oxo-4-phenylbutanoyl)-thiosemicarbazide: Gravimetrical, adsorption and theoretical studies. *Lubricants.* **2021**, *9* (9), 93.
(87) Ben Mahmoud, C.; Anelli, A.; Csanyi, G.; Ceriotti, M. Learning the electronic density of states in condensed matter. *Phys. Rev. B* **2020**, *102* (23), No. 235130.
(88) Lgaz, H.; Lee, H. S. First-principles based theoretical investigation of the adsorption of alkanethiols on the iron surface: A DFT-D3 study. *J. Mol. Liq.* **2022**, *348*, No. 118071.
(89) Jibiao, L.; Shenglong, Z.; Hong, L.; Oguzie, E. E.; Ying, L.; Fuhui, W. Bonding nature of monomeric H2O on Pd: Orbital cooperation and competition. *J. Phys. Chem. C* **2009**, *113* (5), 1931−1938.

https://doi.org/10.1021/acsomega.4c04651
ACS Omega 2024, 9, 38722−38732